A Multimodal Embedded Sensor System for Scalable Robotic and Prosthetic Fingers

Pascal Weiner, Caterina Neef and Tamim Asfour

***Abstract*— The development of dexterous and robust anthropomorphic hands with rich sensor feedback remains a challenging task for both humanoid robotics as well as prosthetics as of today. The design of hands that are scalable in size and equipped with integrated multimodal sensor systems is a key requirement for advanced control schemes and reactive behaviour. In this paper, we present the design of a scalable and low cost robotic finger with a soft fingertip and position, temperature as well as normal and shear force sensors. All cables and sensors are completely enclosed inside the finger to ensure an anthropometric appearance. The finger is modelled based on a 50th percentile male little finger and can be easily adapted to other dimensions in terms of size and sensor system configuration. We describe the design of the sensor system, provide an experimental analysis for the characterization of the different sensor types in terms of sensor range, resolution, creep, spatial response as well as temperature flux.**

I. Introduction

Engineering and construction of anthropomorphic robotic hands remains a challenging task in both humanoid robotics and prosthetics. Perception of modalities such as touch, kinematic state, temperature or vibrations can play a vital role in contact force estimation, slip detection, haptic exploration and object grasping under uncertainties. For both humanoid robotics and prosthetics, anthropomorphic kinematic and appearance are key factors as the hands have to manipulate made-for-humans objects and tools, or, in case of a prosthesis, imitate the natural hand.

The development of tactile sensors for robotic hands and grippers is a very active research field. There exist tactile sensors which measure normal and shear forces as well as tactile sensor arrays with high spatial resolution and accuracy utilizing various measurement principles [1], [2], [3]. Often these sensors require sophisticated fabrication techniques and complex circuitry for signal processing and interpretation which makes them difficult to use as a component in an already complex robotic hand assembly. Therefore it is important to consider specific constraints regarding the whole system when simultaneously designing a tactile or multimodal sensor setup and the hand mechanics [4].

In this work we present the design of a finger for robotic and prosthetic hands with the focus on an anthropomorphic appearance, a flexible multimodal sensor system as well as scalability of the finger and its embedded multimodal sensor system in terms of size and sensor configuration. The finger and its sensor system are designed for use in next versions of our prosthetic hand [5] as well as in the hands of our new humanoid robot ARMAR-6, shown in Fig. 1.

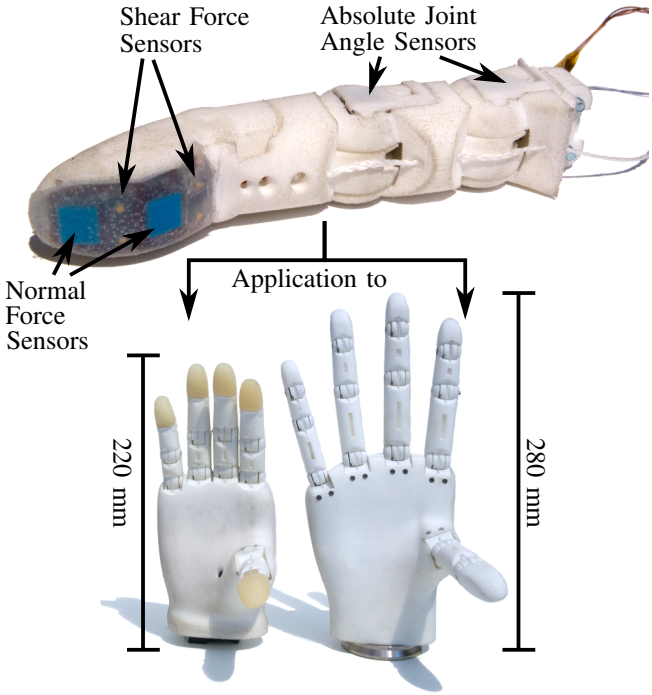

Fig. 1. The finger design with its soft sensorised fingertip (top). The finger with its embedded sensor system is designed with scalability in mind to allow using it in the next versions of our prosthetic hand (left) and the ARMAR-6 hand (right).

The developed finger includes two sensitive normal force and four shear force sensors in the fingertip as well as sensors for joint angle measurement in the proximal interphalangeal (PIP) and metacarpophalangeal (MCP) joint. All sensors are placed on a flexible PCB and are fully integrated in the finger itself. The finger and its embedded sensor system are tested in terms of functionality and accuracy to show the practicability of the design for application in anthropomorphic hands. We consider the anthropomorphic appearance enabled by enclosing cables and sensors in combination with the multimodal sensor system with a soft fingertip the key contribution of this work.

II. Related Work

The design of anthropomorphic fingers and hands requires a close collaboration between multiple disciplines, ranging from mechanical and electrical engineering, material science

This work has been supported by the German Federal Ministry of Education and Research (BMBF) under the project INOPRO (16SV7665) and has received funding from the European Union's Horizon 2020 Research and Innovation programme under grant agreement No 643950 (SecondHands).

The authors are with the High Performance Humanoid Technologies Lab (H^{2}T), Institute for Anthropomatics and Robotics, Karlsruhe Institute of Technology (KIT), Germany, {pascal.weiner, asfour}@kit.edu

to computer science, to guarantee a high degree of hardware and software integration given the constrained space of robotic fingers and hands. Integration of sensors and cables into the mechanical structure of phalanges and joints continues to be a major challenge [2], not least because sensor signals have to be transmitted through miniature joints to a dedicated controller. Quingley et al. [6] utilize steel tendons in the fingers of the Sandia hand for both actuation and digital signal transmission for sensors embedded into the fingertip and phalanges at the expense of additional signal processing electronics. The finger includes optical force sensors, accelerometers and a strain gauge at the PIP joint. For signal transmission in the iHY hand [7] cables are embedded into the phalanges with service loops at the joints. This way tactile feedback from normal force sensor arrays on two phalanges as well as joint angle data based on optical fibre sensors is transmitted to a central controller. Cheng et al. [8] report an underactuated finger design including force and joint angle measurement.

Especially for underactuated hands the measurement of individual finger joint angles is important to estimate the kinematic state of the hand. A number of research hands employ accurate potentiometer based [9] or Hall effect based [10], [11] joint angle sensors implemented directly into the joints. The small space available in anthropomorphic finger joints makes this way of joint angle measurement especially challenging. One way to overcome this problem is to embed IMUs (Inertial Measurement Unit) in the phalanges of the finger and estimate the angle between two IMUs as proposed in [12]. Alternatively combinations of relative encoders on the motors and accelerometers [6] or optical fibre based sensors [7] are used to estimate the finger position. A disadvantage of these methods is the reduced accuracy of the joint angle measurement.

To enable interaction between a robotic hand and its environment, a multimodal sensor system is beneficial to gather information about modalities such as contact, texture, temperature or vibration. In the case of hand prostheses, tactile feedback also plays an important role in dexterous manipulation as it enables the user to modulate grasping forces[13]. The commercially available BioTac fingertip sensor (BioTac, SynTouch Inc.) contains 19 electrodes for contact surface and force estimation, vibration sensing and temperature measurement using a fluid filled soft fingertip ([14], [15]). The fingertip of the humanoid robot iCub utilises flexible printed circuit boards (PCB) to realize a capacitance based normal force sensor array ([16], [17]). To allow an even tighter coupling between mechanical and electrical design, the PCB can be directly printed on a fingertip using a moulded interconnect device (MID) process to form a resistive tactile array as demonstrated by Kõiva et al. [18] and extended by an artificial sensorised fingernail [19] using a MEMS barometer based normal force sensor, a magnetometer based shear force sensor as well as an accelerometer measuring dynamic loads. The development of multimodal sensing systems for robotic hands can be extended for the use in whole body skin [20] and applied to the surface of a humanoid robot [21].

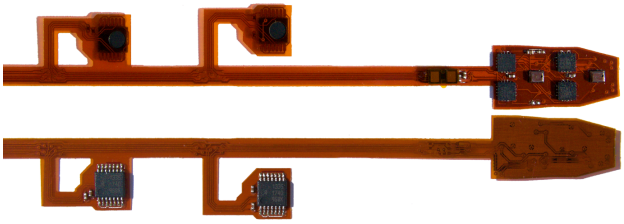

Fig. 2. View of the top and bottom side of the flexible PCB. The part on the right contains six sensors for the fingertip. The two branch-offs accommodate the joint angle encoders. All eight sensors can be connected to a central controller through a common I^2C interface.

III. Embedded Sensor System and Finger Design

The design of the finger is driven by several key requirements. We then transform these into an electromechanical design based on additive manufacturing and state of the art electrical assembly. Sensor design, the PCB as well as the resulting finger joint structure and mechanical assembly are explained in detail in the remainder of this section.

A. Key Requirements

The main objective is to design a robotic finger that can be used in humanoid robotics as well as prosthetics. For both applications the finger has to have anthropomorphic appearance and dimensions. Especially for hand prostheses scalability is important since prosthetic hands and fingers should match the dimensions of the natural hand. Scalability also ensures that the proposed finger design can be transferred to humanoid robotic hands. Sensory and particularly tactile information provides a valuable asset for successful grasping and manipulation of a large variety of everyday objects. For this reason the finger should include a multimodal sensor system that is able to measure normal and shear forces, temperature flux as well as joint angles. As the finger design is meant to be scalable, the sensor system should be easy to customise in terms of arrangement and quantity to support a large variety of different finger segment lengths and fingertip sizes.

B. Embedded Sensor System

All sensors embedded in the finger reside on a common flexible PCB which extends throughout the finger as depicted in Fig. 2. This way the signals of all sensors can be combined and dependably transmitted to a central controller utilizing a common I^2C bus.

The PCB contains two branch-offs at the joints for placement of magnetic absolute encoders (A1335, Allegro MicroSystems LLC) mounted directly on the axis of rotation. A magnet with a $2.5\,\mathrm{mm}$ diameter is mounted on the axis and rotates relative to the absolute encoder.

Six tactile sensors at the fingertip, shown in Fig. 3, provide normal force, shear force and temperature data. Since the sensor system should be easily customisable and the space inside the fingertip is strongly constrained, small digitalised sensor modules are favoured.

We employ 3D shear force sensors as described by Tomo et al. [22], [23]. These sensors utilize a 3D Hall

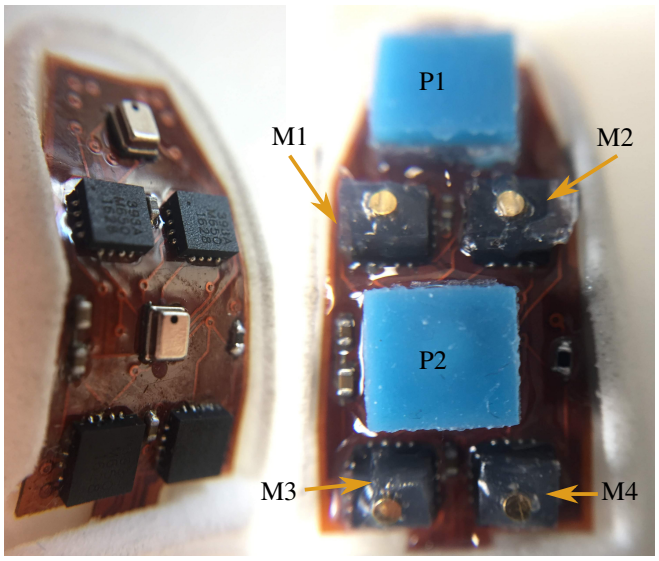

Fig. 3. View of the uncast (left) and partially cast (right) fingertip. Four Hall effect sensors M1-M4 together with their magnets as well as two pressure sensors P1, P2 are cast in flexible silicone rubber that deforms when forces are exerted on it.

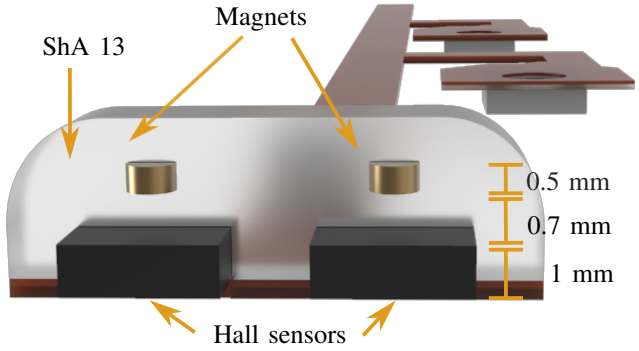

Fig. 4. Cross section of the shear force sensor system, with Hall effect based sensors and magnets placed above them cast in silicone rubber. When a force is exerted on the elastic material, the magnet moves relative to the sensor changing the magnetic field strength and therefore the sensor output values.

effect based digital sensor (MLX90393, Melexis) and corresponding magnet enclosed in flexible material. The magnet is positioned above the sensor floating in the flexible material, as shown in Fig. 4. When a force is applied to the material, the magnet changes position relative to the sensor. We use an N45 magnet with a diameter of $1\,\mathrm{mm}$ and a height of $0.5\,\mathrm{mm}$ in combination with a silicone with Shore A (ShA) hardness of 13. The magnet is positioned $1.2\,\mathrm{mm}$ above the sensing element. Four of these sensors are spread out on the fingertip.

For various tasks like haptic exploration or dexterous manipulation very sensitive force sensing elements are beneficial. Since the above described shear force sensors exhibit a reported normal force resolution of around $0.1\,\mathrm{N}$ depending on the sensor settings, a second sensor technology is embedded into the fingertip to explicitly measure normal forces. These sensors are inspired by the MEMS barometer based normal force sensors developed by Tenzer et al. [24]

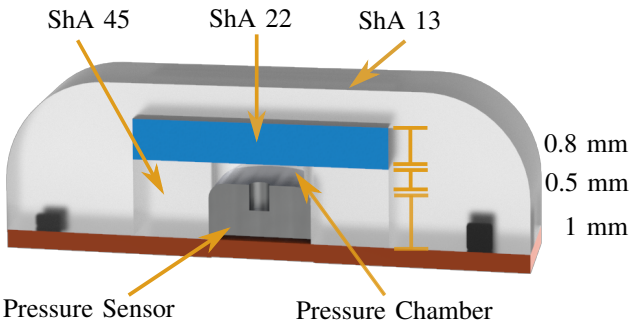

Fig. 5. Cross section of the normal force sensor including a pressure sensor cast in a material of ShA hardness 45 that includes a pressure chamber, and another layer of ShA 22. In a final step, the sensor system along with the rest of the fingertip is cast in ShA 13 material. When a force is exerted onto the elastic material, the pressure in the pressure chamber and therefore the sensor output increases.

which were subsequently used in the iHY hand [7]. While Tenzer et al. cast a $3 \times 5\,\mathrm{mm}^2$ sensor in polyurethane rubber using vacuum degassing to ensure the material flow into the sensor casing, we cast a significantly smaller $2 \times 2.5\,\mathrm{mm}^2$ sensor (NPA 201, Amphenol Advanced Sensors) in three layers of silicone rubber that include a pressure chamber above the sensor casing, which is shown in Fig. 5. The first layer ($1.5\,\mathrm{mm}$, ShA hardness 45, transparent) is less elastic to provide a base for the more elastic material that is to be deformed, and includes a cylindrical pressure chamber ($2\,\mathrm{mm}$ diameter, $0.5\,\mathrm{mm}$ height) directly above the hole of the sensor casing through which the pressure is measured. The second layer ($0.5\,\mathrm{mm}$, ShA hardness 22, blue) is more elastic so that a force exerted upon it deforms the material and increases the pressure in the pressure chamber of the first layer. The third layer with ShA hardness 13 then encloses the whole fingertip.

The sensors are arranged into an alternating pattern beginning with two shear force sensors, M3 and M4, left and right of the centre of the fingertip next to the proximal end followed by a normal force sensor P2. This pattern is repeated a second time up to the fingertip with M1, M2 and P1, as shown in Fig. 3. One normal force sensor (P1) is placed at the fingertip to enable fine-grained control when using the fingertip to pick up small objects and use grasps where more precision and less force are needed (e.g. pinch grasps). The second normal force sensor (P2) is positioned at the centre of the finger pad, as this part of the fingertip first comes into contact with objects that are to be grasped using common grasps such as the cylindrical or hook grasp [25]. The Hall sensors are placed left and right of the centre line as their main use is to measure shear forces where the placement at the centre is less important. Furthermore this allows the placement of two sensors next to each other and hence doubles the amount of receivable information in the constrained space.

The normal force sensors are also used to measure temperature, from which information regarding temperature flux between the sensorised fingertip and the material it is in contact with can be deduced. Although both pressure and Hall

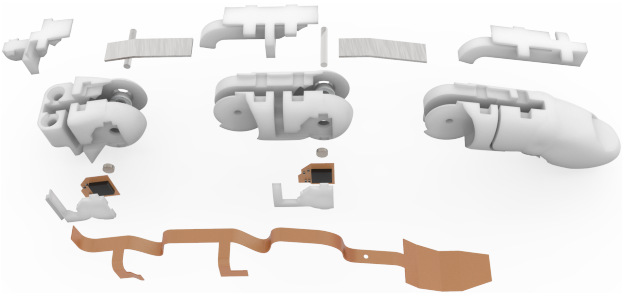

Fig. 6. Explosion view of the developed finger. The cable funnel inside the finger as well as the magnetic encoders at the joints are hidden by two covers at each phalanx. In this view, the PCB is separated at the encoder branch-offs to better show the assembly of the encoders at the joints.

effect sensors are able to measure temperature, the pressure sensors allow a more streamlined bus communication while achieving sufficiently reliable and accurate measurements. When sending a measurement command to the pressure sensor, both temperature and pressure data is automatically measured and returned, whereas the Hall effect based sensors require two additional bytes to be sent when the temperature value is also requested. Therefore, using the pressure sensors for thermal information leads to less data being transferred on the bus. Additionally, the materials used in the fingertip conduct temperature well as all sensors reside on a common ground plane, leading to a similar temperature throughout the entire fingertip.

The part of the flexible PCB containing the six tactile sensors is glued into the fingertip and bends along its surface. The individual sensors, including mounted magnets and pressure chambers, are cast into a common enclosing layer of silicone (ShA hardness value of 13) to protect them and grant the fingertip a smooth and soft surface. This is beneficial for both grasp stability and compliance [26]. Due to the high friction coefficient of soft silicone, the fingertip also grants additional grip during grasping.

C. Mechanical Design

The finger sizing in all dimensions corresponds to a little finger in a 50^{th} percentile male hand according to the German standard specification (DIN 33402-2). As this standard only includes the sizing of the finger as a whole, individual finger segment lengths are based on the human hand reference model of the Master Motor Map [27] and fine-tuned based on recent studies [28]. Fig. 6 shows all mechanical finger parts and in particular the placement of the flexible PCB inside the finger. The PCB forms service loops inside both joints in order to allow the joints to move without damaging the electronics. Special care was taken to keep the signal traces on a single layer as well as in a straight line at all bending parts of the PCB to minimise the bending radius. Vias were only placed on parts of the PCB that do not bend to minimise the chance of a signal fault.

The finger includes two joints which are actuated by a common tendon for flexion at the palmal of the phalanges. The finger is extended by a stack of three stainless steel leaf springswith $100\,\mu\text{m}$ thickness, which are positioned above

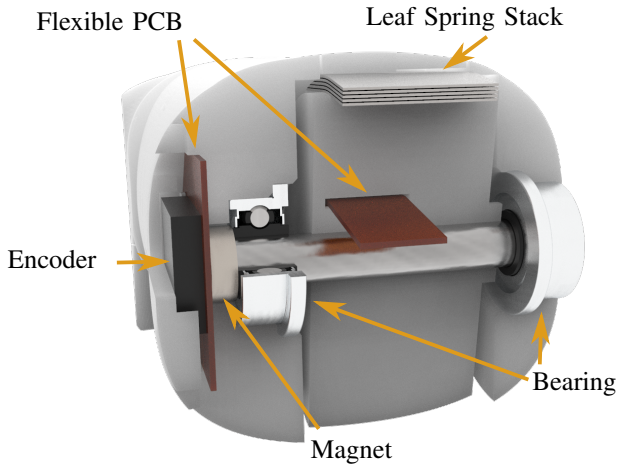

Fig. 7. Cross section view through the PIP joint. On the left side a magnetic encoder and corresponding magnet are mounted. At the top a stack of leaf springs provides the necessary torque for finger extension. The PCB runs through the middle of the joint to the fingertip.

the joints on the dorsal side. The joints are supported by miniature ball bearings for minimised friction. The structure of the joint can be seen in Fig. 7.

Special attention was given to the outer appearance of the finger. All cables and sensors are hidden inside the mechanical structure. This does not only lead to a more anthropomorphic appearance but also improves robustness against external influences. To allow assembly of the flexible PCB into both phalanges, the intermediate and the proximal phalanx are split into three parts each. The part on the dorsal side of the phalanx fixates the PCB inside the finger and pre-bends the service loops at the joints. This part also contains the leaf springs. Additional parts at the side of the finger protect and conceal the part of the PCB leading to the joint angle encoders as well as the encoders themselves. All structural parts are 3D-printed by selective laser sintering out of PA2200 to allow for easy production of different finger sizes. The complete finger assembly costs around $135\,€$, where cost can be significantly reduced for higher quantities.

IV. Performance Evaluation

All sensors embedded into the finger are tested individually with respect to key sensor parameters. We furthermore test the interplay of the different sensors by means of a spatial mapping of the fingertip. Additionally, we examine the response of the sensorised fingertip to various temperature gradients.

A. Joint Angle Encoders

Since the magnet utilised for the joint angle measurement has a diameter of only $2.5\,\text{mm}$, which is less than half the size of the magnet recommended by the manufacturer, special care was taken to confirm proper sensor output. Therefore, we recorded the motions of a test finger with attached absolute encoders using a passive marker based optical tracking system (VICON MX system with 10 T10 and 4 Vero cameras, 100 Hz, VICON Motion Systems Ltd.). We

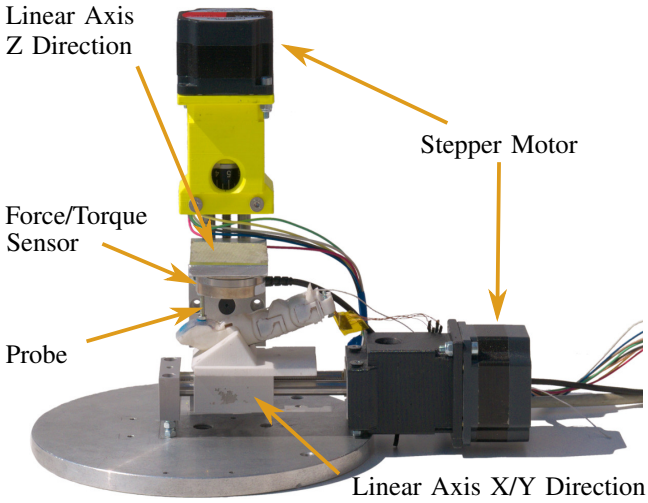

Fig. 8. Overview of test setup with the linear stages, stepper motors, force/torque sensor, the probe and the fingertip shown.

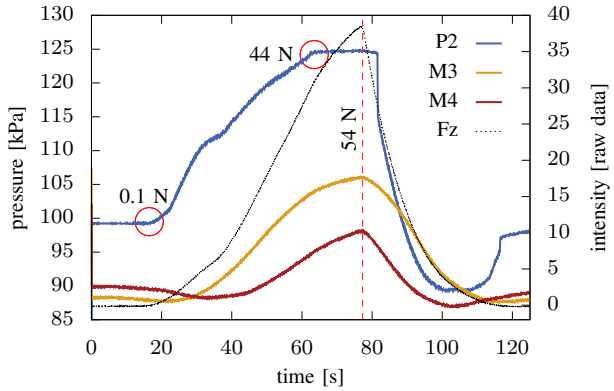

Fig. 9. Response of P2, M3 and M4 to an increasing normal force with a maximum of 54 N (measured by the f/t sensor). The pressure sensor values of P2 begin at approximately 100 kPa, as this corresponds to the atmospheric pressure. P2 reacts first at 0.1 N and saturates at 44 N, while M3 and M4 continue to show a response. Fz of the f/t sensor is plotted for qualitative reference only.

then compared the recorded trajectories to the measurements of the sensors. Even during erratic motions, 85.95 % of all measurements show absolute measurement errors below 3° and during motion speeds normally occurring in robotic hands all measurement errors are below 3°.

B. Test Setup

For experiments conducted to determine sensor characteristics such as range and spatial response, we use a calibrated force/torque sensor (Mini 40, ATI Industrial Automation) and two linear stages (PT4808, MM Engineering GmbH) controlled by stepper motors for increased accuracy (min. step size corresponds to 0.005 mm). One linear stage is mounted in z (vertical) direction, while the other is mounted in either x or y (horizontal) direction for shear force tests. A probe is screwed onto the force/torque sensor which is mounted on the linear axis that is moveable in z direction. The complete setup can be seen in Fig. 8. When this probe is placed above a sensor and the linear z-axis is moved downwards, the exerted forces are measured by the force/torque sensor and can be used to correlate normal force and shear force sensor outputs.

C. Individual Sensor Characterisation

For normal force resolution measurement of both barometer and Hall effect based force sensors calibrated weights were used. The barometer based tactile sensors are able to discriminate weights as low as 0.5 g while the Hall effect based tactile sensors show a resolution of 50 g. The range was determined using the previously described test setup and a probe with a diameter of 5.3 mm. The barometer based sensors saturate at about 6.75 N while the normal force measurement of the Hall effect based sensors saturates above 15 N. The difference in sensitivity and range for both sensor types is shown in Fig. 9. A continuously increasing force was applied up to a maximum of 54 N using a probe with a diameter of 12 mm to ensure contact with both the pressure sensor (P2) and the Hall sensors (M3 and M4). The pressure sensor reacts to the exerted force (around 16.5 s) before the Hall sensors, confirming its higher sensitivity. However, P2 saturates at around 63.5 s and 44 N when it reaches 126 kPa, while the Hall sensors continue to respond to the force. Since pressure decreases with increasing contact area when exerting the same force, the saturation force depends on the contact area of the probe/object that is in contact with the fingertip. Due to the larger contact area with this probe, the sensor reaches saturation at a higher force than in previous tests. When the force is removed, the pressure drops suddenly because the silicone sticks to the probe, causing underpressure. The experiment results confirm the benefits of combining both sensor types, as the pressure sensor exhibits higher sensitivity while the Hall sensors have a wider range.

To measure the shear force resolution, an empty cup weighing 10 g was tangentially pressed against the fingertip with a force of 1 N measured by the f/t sensor. Weights of 4.6 g were incrementally added. The sensor response for the sensors M1 and M2 can be seen in Fig. 10. Each step is clearly distinguishable as the addition of each weight leads to a local peak in the measured shear force resulting from falling into the cup, followed by a plateau indicating the added shear force. M2 exhibits a stronger excitation as the cup is conical in shape and therefore pressed more firmly against the upper sensor M2 than M1.

The influence of the viscoelastic material in terms of creep on both sensor types is examined in Fig. 11. Using the described test setup, a displacement into the elastic material of 1 mm (resulting in a maximum force of 5 N) for the pressure sensor and 2 mm (resulting in 10 N) for the Hall effect based sensor is applied and held for 120 s. While the force measured by the f/t sensor decreases in both cases, the values measured by the normal and shear force sensors exhibit a visibly stronger reduction in signal strength.

D. Tactile System Evaluation

To evaluate the sensor systems' ability to determine thermal flux, four different materials, i.e. wood, PVC, aluminium

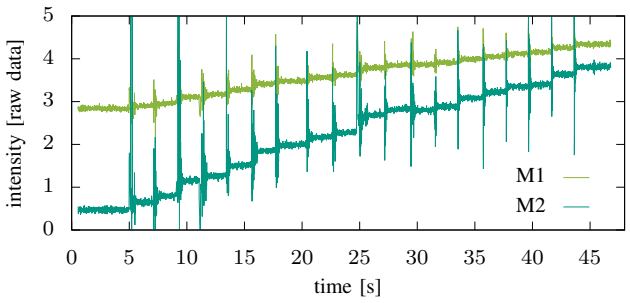

Fig. 10. Results of shear force tests where 4.6 g weights were added incrementally to an empty container pressed laterally against the sensorised fingertip. The resulting increase in shear force for each step can clearly be seen. The spikes mark the moment where the weights where dropped into the container.

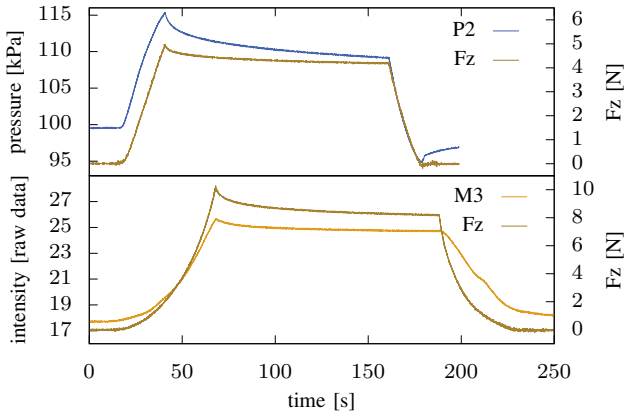

Fig. 11. Creep behaviour of both pressure and Hall sensors cast in silicone rubber. A force of 5 N for P1 and 10 N for M3 is exerted over a period of 120 s and then released. The influence of creep is visible in the overshoot and slow return to the neutral position.

and steel, were placed in the freezer at about −20 °C. Immediately after removal from the freezer the temperature of each material was monitored by placing the finger with the back sensor (P2) directly on its surface. The resulting temperature curves are shown in Fig. 12. Each material was measured until the temperature reached a constant value. As expected, wood shows the smallest impact on the sensor temperature because of its low thermal conductivity, while steel had the highest impact. The experiment shows that the fingertip is able to discriminate various strengths of thermal flux. This also helps recognizing high temperatures before the sensors are damaged, as the silicone withstands temperatures up to 200 °C and high flux is detected in seconds.

To test the spatial resolution and interaction between the different sensors, the fingertip was probed from the centre of the proximal end of the sensorised area (M3 and M4) to the centre of the distal end (P1) using a probe with 5.3 mm in diameter in intervals of 0.5 mm. At each contact point 7 N of normal force were applied and all sensors were sampled at the same time. The probe trajectory and results can be seen in Fig. 13. The Hall effect based sensors (M1-M4) show a broad spatial response while the barometer based sensors (P1 and P2) show a sharply bounded spatial response. The two proximal shear force sensors (M3 and M4) exhibit a smaller signal response to the probe than the distal sensors (M1 and

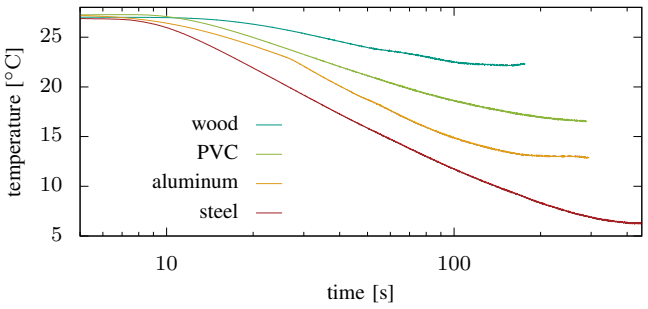

Fig. 12. Temperature flux for various materials, taken out of the freezer at −20 °C and immediately measured using the temperature sensing element included in the pressure sensor. Depending on the thermal conductivity and capacity the material is able to cool the fingertip down to a varying degree. Contact with wood shows the smallest response as it has the lowest thermal conductivity, while steel shows the largest response. The time is plotted using a logarithmic scale.

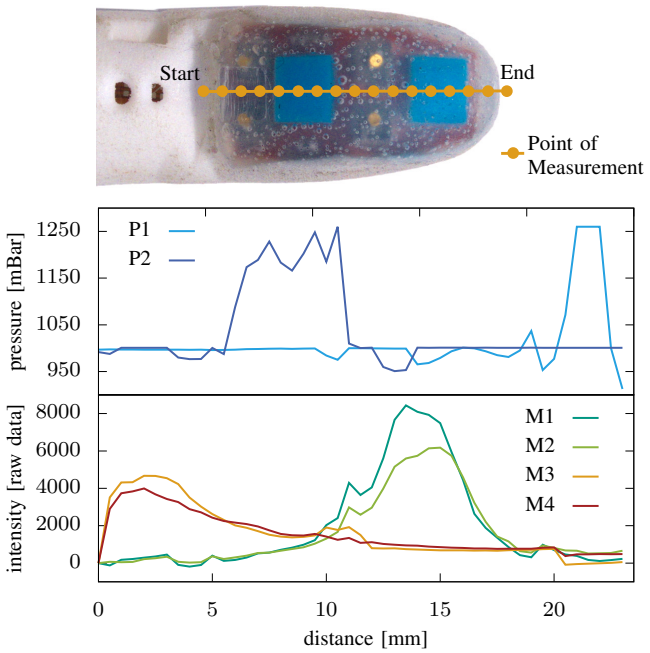

Fig. 13. The top image shows the trajectory of the probe on the fingertip surface from the proximal to the distal end (number of points is qualitative only). A probe with 5.3 mm in diameter was used and 7 N force exerted at each measurement point which where 0.5 mm apart. The plot visualises the sensor response. Due to the positioning of the six tactile sensors, measurements throughout the entire length of the fingertip are possible.

M2). This is most likely due the adjacency to the 3D-printed material at the end of the soft surface which prohibits the flexible material from deflecting in this direction.

V. Conclusion

In this paper we present the design and evaluation of a scalable anthropomorphic finger including a multimodal sensor system embedded in a soft fingertip and miniature joints. The embedded sensor system is completely concealed inside the mechanical structure of the finger. All sensors are embedded on a common flexible PCB which spans the whole length of the finger. This mechatronic design can be used as a blueprint allowing the construction of fingers with

various mechanical dimensions and degrees of sensorisation for both robotic and prosthetic hands. Care was taken to use miniaturised sensors with integrated signal conditioning circuits in combination with standard production processes. This way the sensor system can easily be manufactured and adapted to different finger geometries. The flexible PCB also easily allows reconfiguration of sensor positions as well as the addition of further tactile sensors or additional sensor modalities, as only the PCB layout needs to be adapted. This presents a trade-off in terms of sensor system capabilities in comparison to more integrated approaches like the BioTac sensor fingertip in favour of easy adaptability and scalability as well as low cost.

As experiments show, the combination of shear force sensors with high resolution normal force sensors allows the detection of very delicate interactions while simultaneously sensing normal and shear forces in a much wider range. Due to the sensor placement, forces across the whole area of the fingertip can be detected. The absolute joint angle sensors provide precise measurement of the finger position which is especially important for underactuated mechanisms. The tactile sensor signals are influenced by material creep which is induced by the use of flexible material with a low ShA hardness. This poses a difficult balance between sensor signal clarity and mechanical benefits during grasping which we would like to examine and optimise in future versions. Currently, the sample rate of the used sensors is not sufficient to allow a precise detection of slip events. The addition of sensors with a higher bandwidth like accelerometers in the tip of the finger could help fill this gap.

ACKNOWLEDGMENT

The authors would like to thank Florian von Bertrab for his help with the implementation of the mechanics of the finger joints and absolute encoders, Philippe Spoden for the implementation of the shear force sensors and Samuel Rader for his valuable help with the mechanical construction.

REFERENCES

[1] Z. Kappassov, J.-A. Corrales, and V. Perdereau, "Tactile sensing in dexterous robot hands — review," *Robotics and Autonomous Systems*, vol. 74, no. 1, 2015.

[2] A. Saudabayev and H. A. Varol, "Sensors for robotic hands: A survey of state of the art," *IEEE Access*, vol. 3, no. 0, 2015.

[3] C. Lucarotti, C. M. Oddo, N. Vitiello, and M. C. Carrozza, "Synthetic and bio-artificial tactile sensing: A review," *Sensors*, vol. 13, no. 2, pp. 1435–1466, 2013.

[4] R. S. Dahiya, G. Metta, M. Valle, and G. Sandini, "Tactile sensing - from humans to humanoids," *IEEE Transactions on Robotics*, vol. 26, no. 1, Feb 2010.

[5] P. Weiner, J. Starke, F. Hundhausen, J. Beil, and T. Asfour, "The kit prosthetic hand: Design and control," in *2018 IEEE/RSJ Int. Conf. on Intelligent Robots and Systems (IROS)*, Okt 2018, to be published.

[6] M. Quigley, C. Salisbury, A. Y. Ng, and J. K. Salisbury, "Mechatronic design of an integrated robotic hand," *The Int. Journal of Robotics Research*, vol. 33, no. 5, 2014.

[7] L. U. Odhner, L. P. Jentoft, M. R. Claffee, N. Corson, Y. Tenzer, R. R. Ma, M. Buehler, R. Kohout, R. D. Howe, and A. M. Dollar, "A compliant, underactuated hand for robust manipulation," *The Int. Journal of Robotics Research*, vol. 33, no. 5, 2014.

[8] M. Cheng, L. Jiang, F. Ni, S. Fan, Y. Liu, and H. Liu, "Design of a highly integrated underactuated finger towards prosthetic hand," in *2017 IEEE Int. Conf. on Advanced Intelligent Mechatronics (AIM)*, July 2017, pp. 1035–1040.

[9] L. Wang, J. DelPreto, S. Bhattacharyya, J. Weisz, and P. K. Allen, "A highly-underactuated robotic hand with force and joint angle sensors," in *2011 IEEE/RSJ Int. Conf. on Intelligent Robots and Systems*, Sept 2011, pp. 1380–1385.

[10] T. Asfour, J. Schill, H. Peters, C. Klas, J. Bücker, C. Sander, S. Schulz, A. Kargov, T. Werner, and V. Bartenbach, "ARMAR-4: A 63 DOF Torque Controlled Humanoid Robot," in *IEEE/RAS International Conference on Humanoid Robots (Humanoids)*, Atlanta, USA, October 2013, pp. 390–396.

[11] C. Cipriani, M. Controzzi, and M. C. Carrozza, "The smarthand transradial prosthesis," *Journal of NeuroEngineering and Rehabilitation*, vol. 8, no. 1, p. 29, May 2011.

[12] G. Santaera, E. Luberto, A. Serio, M. Gabiccini, and A. Bicchi, "Low-cost, fast and accurate reconstruction of robotic and human postures via imu measurements," in *2015 IEEE Int. Conf. on Robotics and Automation (ICRA)*, May 2015, pp. 2728–2735.

[13] S. Raspopovic *et al.*, "Restoring natural sensory feedback in real-time bidirectional hand prostheses," *Science translational medicine*, vol. 6, no. 222, pp. 222ra19–222ra19, 2014.

[14] N. Wettels, L. M. Smith, V. J. Santos, and G. E. Loeb, "Deformable skin design to enhance response of a biomimetic tactile sensor," in *2008 2nd IEEE RAS EMBS Int. Conf. on Biomedical Robotics and Biomechatronics*, Oct 2008, pp. 132–137.

[15] J. A. Fishel, V. J. Santos, and G. E. Loeb, "A robust micro-vibration sensor for biomimetic fingertips," in *2008 2nd IEEE RAS EMBS Int. Conf. on Biomedical Robotics and Biomechatronics*, Oct 2008, pp. 659–663.

[16] N. Jamali, M. Maggiali, F. Giovannini, G. Metta, and L. Natale, "A new design of a fingertip for the icub hand," in *2015 IEEE/RSJ Int. Conf. on Intelligent Robots and Systems (IROS)*, Sept 2015, pp. 2705–2710.

[17] A. Schmitz, M. Maggiali, L. Natale, B. Bonino, and G. Metta, "A tactile sensor for the fingertips of the humanoid robot icub," in *2010 IEEE/RSJ Int. Conf. on Intelligent Robots and Systems*, Oct 2010, pp. 2212–2217.

[18] R. Kõiva, M. Zenker, C. Schürmann, R. Haschke, and H. J. Ritter, "A highly sensitive 3d-shaped tactile sensor," in *2013 IEEE/ASME Int. Conf. Advanced Intelligent Mechatronics*, July 2013, pp. 1084–1089.

[19] R. Kõiva, T. Schwank, G. Walck, R. Haschke, and H. J. Ritter, "Mechatronic fingernail with static and dynamic force sensing," in *2018 IEEE/RSJ Int. Conf. on Intelligent Robots and Systems (IROS)*, Okt 2018, to be published.

[20] P. Mittendorfer and G. Cheng, "Humanoid multimodal tactile-sensing modules," *IEEE Transactions on Robotics*, vol. 27, no. 3, June 2011.

[21] E. Dean-Leon, B. Pierce, F. Bergner, P. Mittendorfer, K. Ramirez-Amaro, W. Burger, and G. Cheng, "Tomm: Tactile omnidirectional mobile manipulator," in *2017 IEEE Int. Conf. on Robotics and Automation (ICRA)*, May 2017, pp. 2441–2447.

[22] T. P. Tomo, W. K. Wong, A. Schmitz, H. Kristanto, A. Sarazin, L. Jamone, S. Somlor, and S. Sugano, "A modular, distributed, soft, 3-axis sensor system for robot hands," in *2016 IEEE-RAS 16th Int. Conf. on Humanoid Robots (Humanoids)*, Nov 2016, pp. 454–460.

[23] T. P. Tomo, A. Schmitz, W. K. Wong, H. Kristanto, S. Somlor, J. Hwang, L. Jamone, and S. Sugano, "Covering a robot fingertip with uskin: A soft electronic skin with distributed 3-axis force sensitive elements for robot hands," *IEEE Robotics and Automation Letters*, vol. 3, no. 1, Jan 2017.

[24] Y. Tenzer, L. P. Jentoft, and R. D. Howe, "The feel of mems barometers: Inexpensive and easily customized tactile array sensors," *IEEE Robotics Automation Magazine*, vol. 21, no. 3, Sept 2014.

[25] N. Kamakura, M. Matsuo, H. Ishii, F. Mitsuboshi, and Y. Miura, "Patterns of static prehension in normal hands," *American Journal of Occupational Therapy*, vol. 34, no. 7, pp. 437–445, 1980.

[26] K. Or, S. Morikuni, S. Ogasa, S. Funabashi, A. Schmitz, and S. Sugano, "A study on fingertip designs and their influences on performing stable prehension for robot hands," in *2016 IEEE-RAS 16th Int. Conf. on Humanoid Robots (Humanoids)*, Nov 2016, pp. 772–777.

[27] C. Mandery, O. Terlemez, M. Do, N. Vahrenkamp, and T. Asfour, "Unifying representations and large-scale whole-body motion databases for studying human motion," *IEEE Transactions on Robotics*, vol. 32, no. 4, pp. 796–809, August 2016.

[28] M. Vergara, M.-J. Agost Torres, and V. Gracia-Ibáñez, "Comparison of dorsal and palmar aspect dimensions of hand anthropometry," *Human Factors and Ergonomics in Manufacturing & Service Industries*, vol. 28, no. 1, pp. 1–12, 2016.